Available online at www.sciencedirect.com
ScienceDirect
Global and Planetary Change 55 (2007) 257–272
GLOBAL AND PLANETARY CHANGE
www.elsevier.com/locate/gloplacha

# Interannual sea level variability in the South China Sea and its response to ENSO

Zengrui Rong [a,*], Yuguang Liu [a], Haibo Zong [a], Yongcun Cheng [a,b]

[a] *Physical Oceanography Laboratory, Ocean University of China, Qingdao, 266003, PR China*
[b] *Institute of Meteorology, PLA University of Science and Technology, Nanjing, 211101, PR China*

Received 13 June 2006; received in revised form 9 August 2006; accepted 10 August 2006
Available online 27 September 2006

**Abstract**

Sea level observed by altimeter during the 1993–2004 period, thermosteric sea level from 1945 through 2004, and tide gauge records are analyzed to investigate the interannual variability of sea level in the South China Sea (SCS) and its relationship with ENSO (El Niño and Southern Oscillation). Both the interannual variations of the observed sea level and the thermosteric sea level are closely related to ENSO. An 'enigma' that the SST and sea level in the SCS have inverse response to ENSO is revealed. It is found that the thermosteric sea level has an excellent correspondence to seawater temperature at 100 m depth, and their variations are unsynchronized to SST. Detailed analysis denotes that the warming of seawater occurs only in the upper 75 m during and after the mature phase of El Niño, while the cooling appears in the layers deeper than 75 m during El Niño years. The volume transports between the SCS and the adjacent oceans and the anomalous Ekman pumping contribute a lot for the sea level fall in the developing stage of El Niño, while the mass exchange, which is dominated by precipitation, plays a more significant role in the following continuous negative sea level anomalies.


*Keywords:* interannual variability; South China Sea; sea level anomalies; thermosteric sea level; ENSO; mass exchange

## 1. Introduction

The South China Sea (SCS) is the largest marginal sea in Southeast Asia as shown in Fig. 1. It is a semi-closed basin surrounded by South China, the Philippines, Borneo Island, and the Indo China Peninsula. Water can exchange with the East China Sea, the western Pacific and the Indian Ocean through the Taiwan Strait, the Luzon Strait and the Malacca Strait, respectively. Because of its geographical location, the sea surface temperature (SST) in the SCS is closely related to ENSO (Klein et al., 1999; W. Wang et al., 2000; C. Wang et al., 2006). Possible mechanisms have also been widely discussed (Klein et al., 1999; Wang, 2002; Qu et al., 2004; Wang et al., 2006). The influence of ENSO on the SCS SST is considered to be through the atmospheric bridge of atmospheric circulations. Compared to SST, investigations of sea level in the SCS have mainly been focused on seasonal scale (Ho et al., 2000a; Liu et al., 2001; Hu et al., 2001; Li et al., 2003). Based on 6 years of TOPEX/Poseidon altimeter data, Hwang (2001) noted that the interannual variation of the SCS sea level anomalies is correlated with ENSO. Ho et al. (2000b) successfully identified a third EOF mode (occupied 10% variance) that is related with El Niño. Based on Modular Ocean Model version 2, Qu et al. (2004) investigated the upper-layer heat

* Corresponding author. Fax: +86 532 82032471.
*E-mail address:* rongzengrui@yahoo.com.cn (Z. Rong).

0921-8181/$ - see front matter © 2006 Elsevier B.V. All rights reserved.
doi:10.1016/j.gloplacha.2006.08.001

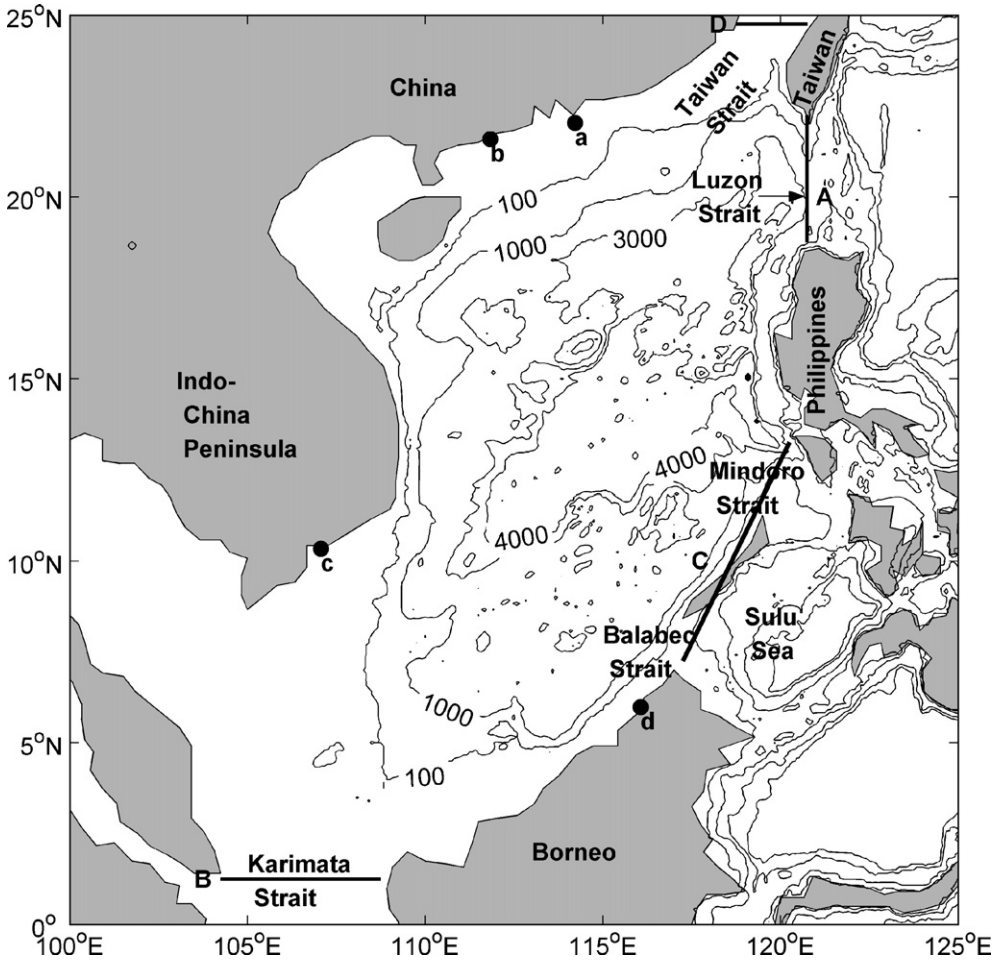


Fig. 1. The bottom topography of the South China Sea and the straits between the SCS and the adjacent oceans.

content in the SCS and a strong signature of ENSO is detected.

Until now, our understanding of interannual sea level variability in the SCS is still very poor. In particular, the mechanisms that are responsible for the SCS interannual sea level variations are not clear. SST anomalies are found to be increased during and after the mature phase of El Niño (Klein et al., 1999; W. Wang et al., 2000; C. Wang et al., 2006). However, since SST data reflects mainly the sea surface thermal phenomena, deep layer water temperature must be investigated in order to enhance our understanding obtained from interpretation of altimeter observations. The main purpose of this study is to examine the interannual variability of the SCS sea level and its relationship with ENSO. We first examine the sea level response to the 1997–1998 warming event and the La Niña event of 1999–2000. For this purpose, we calculate the thermosteric contribution to sea level observed by satellite altimeter, considering the 12 years of overlap between the altimeter mission and the recently released global ocean temperature dataset (Ishii et al., 2003, 2006). Then we analyze the interannual variability of seawater temperature and thermosteric sea level in the SCS during previous decades (1945–2004). Finally, sea level anomalies derived from tide gauge are used to study the correlation with ENSO on a longer time scale. Possible mechanisms of the interannual variability were discussed in Section 6. This study extends the results of earlier works and provides new insight on the long term correlation between interannual sea level changes in the SCS and ENSO.

## 2. Data description

### 2.1. Altimeter data

A merged and gridded product of MSLA (Maps of Sea Level Anomaly) produced by AVISO based on TOPEX/Poseidon, Jason 1, and ERS-1 and ERS-2 data

(Ducet et al., 2000) was used here. This product provides sea level anomalies relative to a 7-year mean from 1993 through 1999. It consists of maps produced every 7 days on a 1/3° × 1/3° Mercator grid. This product has been corrected for all geophysical errors. Because the maps contain data from multiple altimeters, they are able to resolve variability on scale as small as 150–200 km with an accuracy of a few centimeters over most of the globe (Ducet et al., 2000). Based on these gridded data from Jan. 1993 through Dec. 2004, we first derived the 12-year mean of sea level anomalies at each grid point to form a new reference surface, and the new time series of sea level anomalies at each grid point was then derived after subtracting the new reference surface. Then the data are used to construct the time series of the monthly mean sea level anomalies.

### 2.2. Historical ocean subsurface temperature dataset

The monthly objectively analyzed subsurface temperature (version 6.2) at 16 levels in the upper 700 m for the period 1945–2005 is the most recently available dataset produced by Ishii et al. (2003, 2006). The analysis is based on the World Ocean Database 2001(WOD01) (Boyer et al., 2001), the Global Temperature–Salinity in the tropical pacific provided by IRD (L'institut de recherché pour le development, France), and the Centennial in situ Observation Based Estimates (COBE) sea surface temperature (Ishii et al., 2005). ARGO-profiling buoy data and the latest GTSPP (Global Temperature–Salinity Profile Program) data have also been used in the final several years. A bug associated with the mixed layer depth analysis has also been fixed (Ishii et al., 2006). The spatial resolution of the data is 1° × 1°, with the time period from 1945 through 2004 was used here.

### 2.3. Thermosteric sea level

It is possible to estimate the thermosteric sea level by using the temperature dataset described above. To compute the thermosteric sea level, i.e. due to temperature only, it is necessary to first convert the gridded temperature anomalies to density anomalies at each depth using the classical equation of state (Gill, 1982). The thermosteric sea level is further obtained by vertically integrating density anomalies at each grid point and each time step according to (e.g. Lombard et al., 2005):

$$h_{\text{steric}}(x,y,t) = \int_{-H}^{0} \frac{\rho_0(x,y,z) - \rho(x,y,z,t)}{\rho_0(x,y,z)} \mathrm{d}z$$

where $\rho_0(x,y,z)$ is the reference density; $\rho_0$ is a function of reference temperature $T_0$ (0° C), reference salinity $S_0$ (Levitus climatology) and depth $z$. $\rho(x,y,z,t)$ is a nonlinear function of temperature and salinity (Gill, 1982). The Levitus climatology is used as the reference salinity at each depth for Ishii temperature dataset.

## 3. The variability of observed and thermosteric sea level in the South China Sea during the period 1993–2004

We first calculate the sea level trends over the period 1993–2004 by fitting at each grid mesh a linear function after removal of the annual and semiannual signals. The geographical distribution of the observed sea level trends is shown in Fig. 2a. Positive sea level trends are found in most part of the basin, only the lower center off the southeast coast of Vietnam is below zero. However, it is evidenced that the sea level trends in the SCS are not homogeneous. The striking character is that a relatively lower sea level trend (below average) lies in the southwest–northeast direction across the central SCS and sea level trends on both sides of it are generally higher than average. Thermosteric sea level change for the overlapping period of 1993–2004 is also available from Ishii temperature dataset. To calculate the trends, a similar method as for the observed sea level is used. Fig. 2b shows the geographical distribution of thermosteric sea level trends for the period 1993–2004. Note that the thermosteric sea level trends are positive all over the basin. A peak center around 18° N, 117.5° E reveals a highest rising rate of 8.5 mm/yr. The observed and the thermosteric sea level trends show obvious differences to each other. This is mainly because non-steric sea level variations obviously exist in the SCS. Water mass redistribution due to water exchange through the water cycle and the oceanic circulation may have significant impacts on altimeter observed sea level change, which are not part and not included in the thermosteric estimate.

To investigate the water mass exchange over the SCS, we simply calculated the regional average of the observed and the thermosteric sea level anomalies over the SCS. Fig. 3 shows the time series of the altimeter observed and Ishii thermosteric sea level anomalies over the SCS and the mass exchange denoted by their difference. The annual fits are also superimposed. Note that both the amplitude and the phase show difference between the observed and thermosteric sea level anomalies. Least squares fits to the data give annual amplitudes of 48 mm and 36 mm for altimeter observation and Ishii thermosteric sea level, respectively. The annual amplitude of the observed sea level is

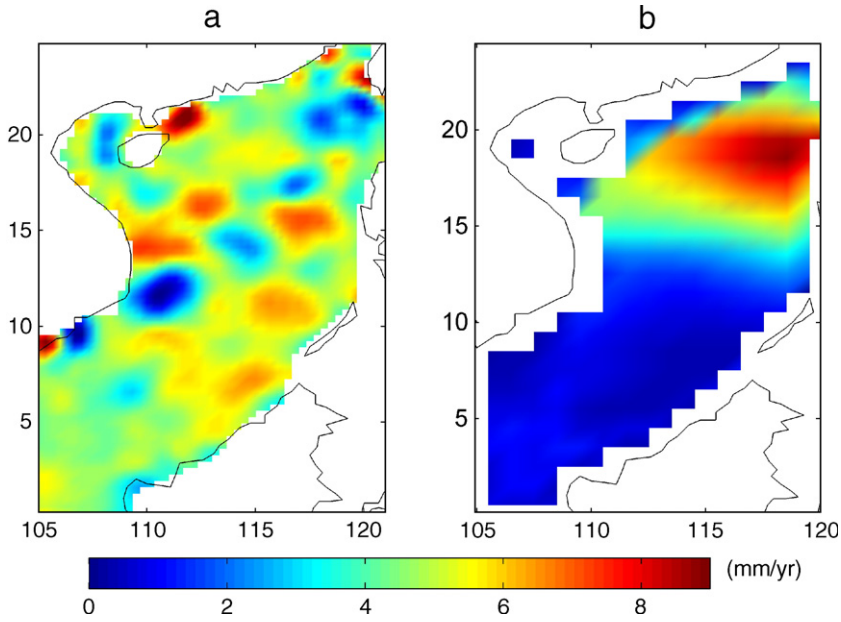


Fig. 2. The observed sea level trends over the SCS (a) and the thermosteric sea level trends (b) in the same area.

12 mm larger than the thermosteric contribution. Also there is a phase difference between them, with the thermosteric sea level leading the observation by 3 months. The sea level variation due to ocean mass exchange is the difference between the altimeter observed sea level and the thermosteric contribution.

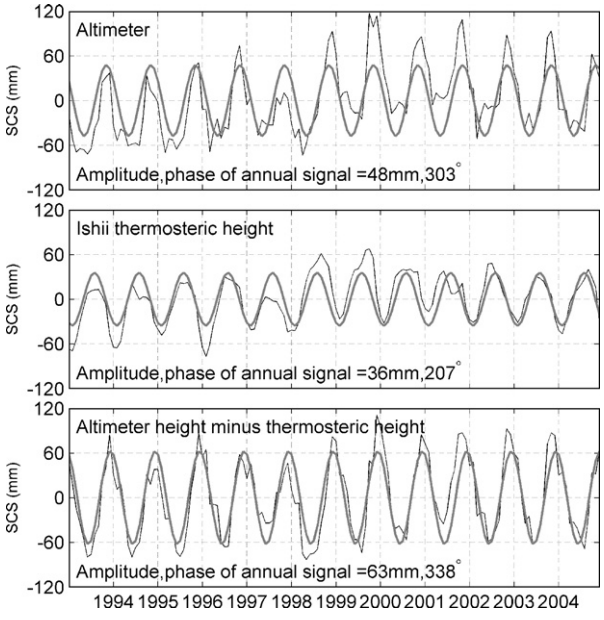


Fig. 3. Time series of the mean sea level anomalies over the SCS (a) altimeter observed sea level variation, (b) thermosteric sea level variation, (c) the mass exchange. Annual fits are superimposed.

The annual variation of the altimeter observed sea level corrected for thermosteric effect has an amplitude of 63 mm with a maximum in December. This variation should result from ocean mass exchange between the atmosphere and the continent via precipitation, evaporation and runoff. Since the SCS is not a closed basin, the water mass exchange between the SCS and the adjacent oceans may also play a role.

Sea level anomalies during the period 1993–2004 may not be dominated by a straightforward trend but rather by interannual fluctuations. It is difficult to visualize the interannual variations of sea level in a plot of monthly means. Seasonal signals are so large and variable that the smaller, longer-period signals are obscured. Thus appropriate filtering is needed for visualization of these signals. In this study, the seasonal signals of the time series were first removed by least squares fits, and then a Butterworth low-pass filter with a cut frequency corresponding to the period of 2 years and order 5 was applied. Fig. 4 shows the low-pass filtered SOI and the observed mean sea level anomalies. As shown in Fig. 4, the curve of the mean sea level anomalies appears dominated by interannual fluctuations, particularly in the period 1997–1998 when the SOI has a minimum (El Niño event) and in the year 1999 when the SOI has a maximum (La Niña event). It is evidenced that the mean sea level anomalies over the SCS are strongly corresponding to ENSO. Sea level anomalies and SOI vary coherently: negative values of the SOI (i.e. El Niño event) correlating with negative sea

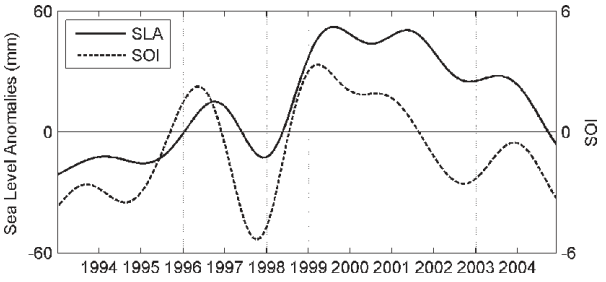


Fig. 4. Comparison of the low-passed mean sea level anomalies in the SCS with the low-passed SOI.

level anomalies and conversely. The correlation between the interannual components (the low-passed components) of the mean sea level anomalies and the SOI reaches 0.78 with SOI leading the mean sea level anomalies by 4 months (see Table 1).

To better describe the spatio-temporal behaviors of the interannual SCS sea level, we performed an empirical orthogonal function (EOF) analysis (Preisendorfer, 1988) over the period 1993–2004 to the gridded monthly sea level anomalies data. The EOF analysis gives a possibility to identify the main patterns of spatial and temporal variability and to evaluate the contribution of different components of variability, as well as to look for significant correlation with the external forcing. Here the seasonal signals were first removed and a Butterworth low-pass filtering the same as above was then applied.

Fig. 5 shows the first mode of the sea level decomposition of the low-pass filtered fields, which accounts for 62% of the total variance. The spatial patterns of the first EOF mode are characterized with the same sign basin-wide, which indicate that they occur synchronously over the whole sea (Fig. 5 top). However, the horizontal

Table 1
Correlation between SOI and the thermosteric sea level anomalies, water temperature anomalies at 100 m depth, the SCS SST anomalies and the observed sea level anomalies. Positive lag indicates a SOI lead. All values are significant at 95% confidence level. The effective degrees of freedom were estimated by using the method proposed by Trenberth (1984)

| | Thermosteric sea level anomalies (1945–2004) | Seawater temperature at 100 m depth (1945–2004) | Sea surface temperature (1945–2004) | Observed sea level anomalies (1993–2004) |
|---|---|---|---|---|
| Correlation | 0.37 (0.53 for 1975–2004) | 0.42 | −0.44 | 0.78 |
| Time lag (month) | −3 (−3 for 1975–2004) | −1 | 5 | 4 |

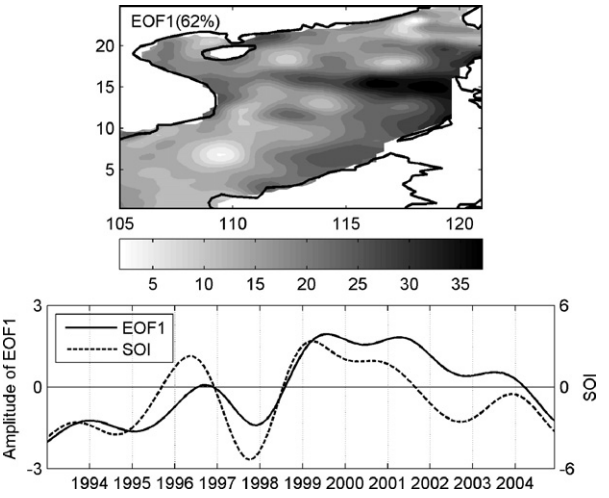


Fig. 5. First EOF mode of the sea level anomalies in the SCS (a) Spatial pattern on top (b) principal component of the low-pass filtered SLA and the low-pass filtered SOI on bottom.

gradients in amplitude are large, and a major signal (high amplitude) is apparent at the southeast part of the SCS, especially along the 15° N and extending to the central Vietnam coast. The bottom panel of Fig. 5 shows the first principal component time series and the SOI. Positive amplitude of the principal component representing higher sea level appears from mid-1998 to the end of 2003. Negative amplitude of the principal component representing lower sea level appears from 1993 to mid-1998. The comparison between the principal component and SOI implies that the interannual variability of the SCS sea level is highly correlated with ENSO. Sea level related to ENSO falls synchronously during El Niño years over the whole sea as denoted the same sign in Fig. 5 top, and a reverse situation takes place during La Niña years.

## 4. Interannual variability of seawater temperature and thermosteric sea level

### 4.1. Interannual temperature variability

The influence of ENSO on the SCS sea surface temperature (SST) has been widely discussed in previous studies (Klein et al., 1999; Wang et al., 2000; Qu et al., 2004; Wang et al., 2006). It is found that SST gets warmer in the SCS during and after the mature phase of El Niño. The influence of ENSO on the SCS SST is believed to be through the atmospheric bridge of atmospheric circulation changes (Klein et al., 1999; C. Wang et al., 1999; W. Wang et al., 2000; Wang, 2002; Wang et al., 2006). During El Niño, convective activity in the equatorial western Pacific shifts eastward. This

shift in convection leads to an altered Walker circulation and an anomalous descent is formed over the western equatorial Pacific, while an anomalous ascent is formed over the eastern Pacific. Thus, the Hadley circulation strengthens over the eastern Pacific but weakens over the Indo–Western Pacific (Klein et al., 1999; Wang, 2002). The SCS lies near the anomalous descent region. Surface wind, air temperature, humidity, and cloud cover were altered there which in turn influence the ocean circulations and surface heat fluxes and eventually SST.

Fig. 6 gives a comparison of the SOI with the SST anomalies in the SCS. In Fig. 6a, the SOI has been multiplied by a factor of −1 to facilitate comparison. The linear trend of SST has been removed, and both SOI and the SST anomalies are time series of 3-month running means (the average of 3 months data). Here we find that the correlation between the SCS SST anomalies derived from Ishii dataset and SOI is −0.44 and is significant at the 95% confidence level, with SOI leading the SCS SST anomalies by 5 months (see Table 1). Every ENSO event is associated with a change of the SCS SST anomalies. The consistency with earlier investigations confirms the accuracy of the dataset and our analysis. We also applied a wavelet coherence analysis (Grinsted et al., 2004) to SOI and the SCS SST anomalies. The wavelet coherence is used to examine the correlation in both frequency bands and time intervals. Fig. 6b shows the wavelet coherence between SOI and the SCS SST anomalies. The SOI and SCS SST anomalies show significant coherence in the 2–7 year periods. A relatively lower coherence is found from 1945 to 1960. Vectors in Fig. 6b indicate the phase difference between the SOI and the SCS SST anomalies at each time and period, with in-phase pointing right, anti-phase pointing left, and SOI leading SCS SST anomalies by 90° pointing straight up (Grinsted et al., 2004). In the 2–7 year periods, the SOI and the SCS SST are approximately 180° out of phase, indicating that warmer SST during El Niño years and colder SST in La Niña years.

It is worth to note that responses of the SCS SST anomalies and the SCS mean sea level anomalies to SOI (i.e. ENSO) are completely out of phase (see Figs. 4 and 6a and correlations in Table 1). The SST reached its maximum with a lag of about 5 months behind the mature phase of El Niño, while the sea level anomalies reached its minimum with a lag of about 4 months.

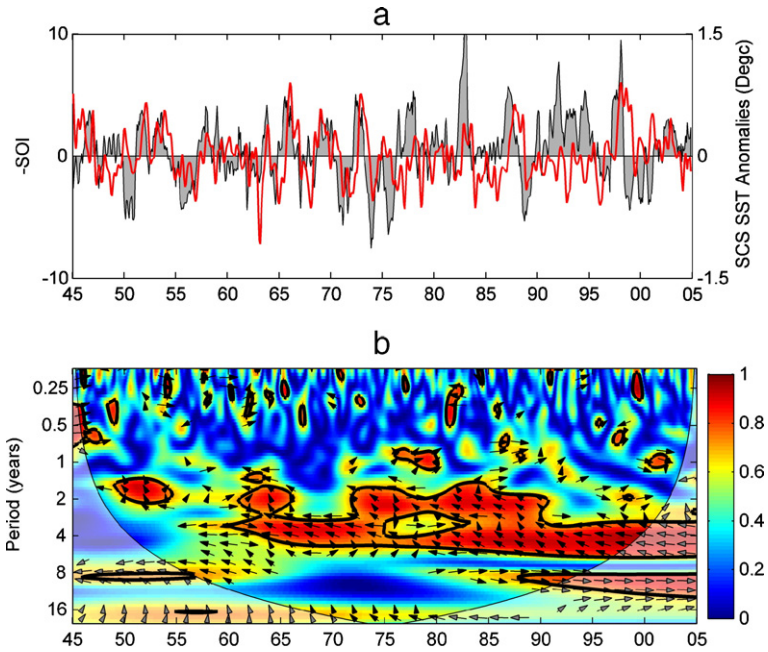


Fig. 6. Comparison of the SOI with the SST anomalies in the SCS (a) the time series of SOI (shaded curve) and SST anomalies (red curve). SOI has been multiplied by a factor of −1 to facilitate comparison. The linear trend of SST has been removed and both time series are 3-month running means. (b) The wavelet coherence and phase relationship between SOI and SCS SST anomalies. The thick black contour is the 5% significance level and the cone of influence where edge effects might distort the picture is shown as a lighter shade. The vectors indicate the relative phase relationship (with in-phase pointing right, anti-phase pointing left, and SOI leading SCS SST anomalies by 90° pointing straight up). (For interpretation of the references to colour in this figure legend, the reader is referred to the web version of this article.)

What's the reason for such an 'enigma'? Since the SST anomalies reflect mainly the sea surface thermal phenomena, deep layer water temperature must be investigated in order to enhance our understanding. To explain this 'enigma', the seawater temperature variations at each depth during the period 1945–2004 are investigated. For each depth, the Ishii seawater temperature anomalies are averaged over the SCS, and a 3-month running mean is then applied to the seawater temperature anomalies. Correlation between temperature anomalies and SOI is then evaluated at each depth. Fig. 7 shows the correlation corresponding to different time lags between seawater temperature anomalies and SOI as a function of depth. While the largest negative correlation of −0.44 between the SST anomalies and SOI is detected, with SOI leading the SST anomalies by 5 months, positive correlations between the temperature anomalies and SOI are detected in all intermediate layers deeper than 75 m. This indicates that while SST and seawater temperature in the upper 75 m are singularly warm, seawater temperatures of intermediate layers (75–700 m) are abnormally cold. The largest positive correlation between the seawater temperatures of intermediate layers and SOI is found to be 0.42 at 100 m depth when the SOI lags the seawater temperature by 1 month (see Table 1), and it is significant at the 95% confidence level. The abnormally colder water in the intermediate layers during El Niño years may account for the negative anomalies of sea level during El Niño years (see Fig. 4).

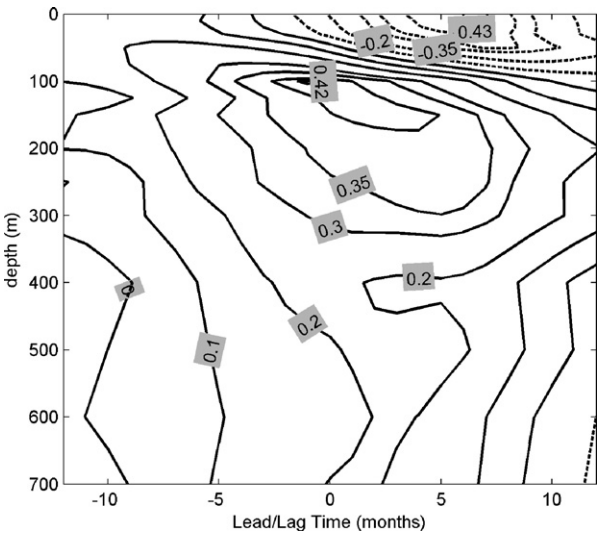


Fig. 7. Correlation corresponding to different time lags as a function of depth between seawater temperature anomalies and SOI. The solid line represents positive correlation, the dashed line represents negative correlation, and the positive lag indicates that the SOI leads the seawater temperature anomalies.

Taking seawater temperature anomalies at 100 m depth as an example of intermediate layers, Fig. 8 gives a comparison of the SOI with the seawater temperature anomalies at 100 m depth in the SCS. In Fig. 8a, both SOI and the seawater temperature anomalies at 100 m depth are time series of 3-month running means. It is found that every ENSO event is associated with a change of the seawater temperature anomalies at 100 m depth, i.e. cooling during El Niño years and warming during La Niña years. Fig. 8b shows the wavelet coherence between the SOI and the SCS seawater temperature anomalies at 100 m depth. Fig. 8b reveals that the most significant coherence occurs in the 2–7 year periods. Also, from 1980 to 2005, there is appreciable coherence at longer periods. Vectors in Fig. 8b indicate that the SOI and the seawater temperature anomalies at 100 m depth have in-phase variation in the 2–7 year periods. Comparing Fig. 6b with Fig. 8b, one will note that the vectors in the 2–7 year periods are approximately in opposite direction. This further reveals that responses of SST and seawater temperature at 100 m depth, as an indication of intermediate layers, to ENSO are reverse.

### 4.2. Interannual thermosteric sea level variability

Responses of seawater temperatures anomalies at intermediate layers to SOI (i.e. ENSO) are different to that of the SST anomalies in the SCS. The question then is: "How does the thermosteric sea level response to ENSO?" In order to answer this question, we further calculate the mean thermosteric sea level anomalies over the SCS from 1945 through 2004 and then try to investigate their correlation with ENSO.

For the 1945–2004 period, the thermal expansion of seawater at the 0–700 m layer of the SCS contributed approximately 0.14 mm/yr to the SCS sea level rise. Fig. 9 gives a comparison of the SOI with the thermosteric sea level anomalies averaged in the SCS, after removing the seasonal signals and the rising trend. The temporal correspondence of the thermosteric sea level anomalies in the SCS to SOI (i.e. ENSO) is striking. The SCS thermosteric sea level is negative during El Niño years, and it changes from below normal to above normal at the end of an El Niño event. Positive anomalies of thermosteric sea level seem to be a common feature in La Niña years. The SCS thermosteric sea level anomalies have a negative minimum around the mature phase of El Niño. The correlation between the SCS thermosteric sea level anomalies and SOI reaches 0.37, with the SCS thermosteric sea level anomalies leading SOI by 3 months.

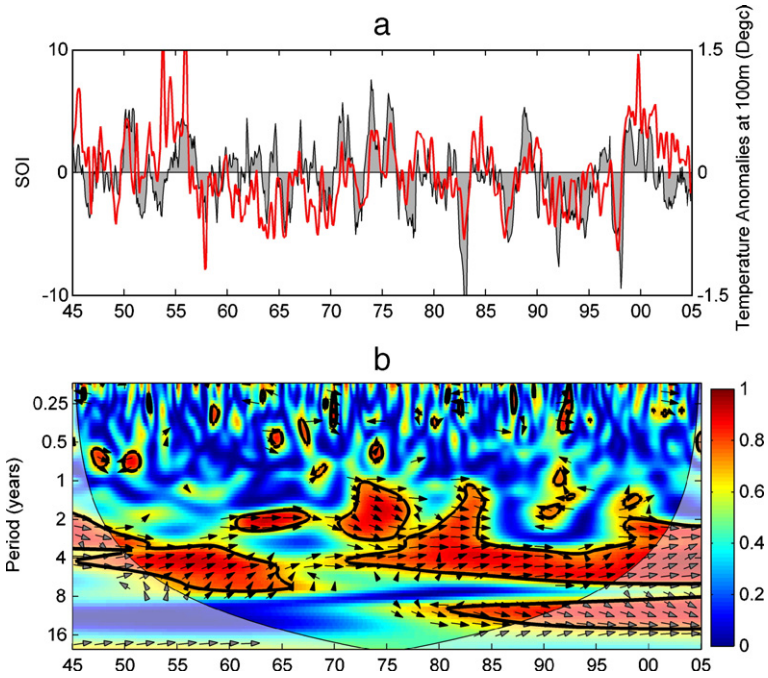


Fig. 8. Comparison of the SOI with the seawater temperature anomalies at 100 m depth in the SCS (a) the time series of SOI (shaded curve) and seawater temperature anomalies at 100 m depth (red curve). The linear trend of seawater temperature has been removed and both time series are 3-month running means. (b) The wavelet coherence and phase relationship between SOI and SCS seawater temperature anomalies at 100 m depth. The thick black contour is the 5% significance level and the cone of influence where edge effects might distort the picture is shown as a lighter shade. The vectors indicate the relative phase relationship (with in-phase pointing right, anti-phase pointing left, and SOI leading seawater temperature anomalies by 90° pointing straight up). (For interpretation of the references to colour in this figure legend, the reader is referred to the web version of this article.)

Furthermore, the correlation does not appear steady in time. The correlation with a SOI lead of 3 months was 0.20 during the 1945–1975 period, and increased to 0.53 during the 1975–2004 period (see Table 1). As shown in Fig. 9b, the coherence is significant in only one band with the periods around 5 years before 1975, while it is also significant at longer periods in the 8–15 year band after 1975. This can explain why the correlation is lower before and higher after 1975. Note that the phase difference has also decreased from about 90° (the upward arrowhead) before 1975 to about 0° (the rightward arrowhead) after 1975, in band with the period around 5 years. The high correlation after 1975 could mean that El Niño had a larger effect on sea level variation.

Comparing Figs. 6, 8 and 9, it is worth to note that the thermosteric sea level anomalies have a good correspondence to seawater temperature anomalies at 100 m depth and are out of phase with SCS SST anomalies. As shown in Fig. 7, seawater temperature at 100 m depth may be an indication of the intermediate layers, i.e. deeper than 75 m. We may deduce that the thermosteric sea level variations are mainly due to temperature variations in the intermediate layers. Seawater temperature anomalies in the upper 75 m can usually be easily explained in terms of local air–sea interaction while mechanisms of the deeper anomalies are more complicated. However, the warming of seawater in the upper 75 m during and after the mature phase of El Niño may have an effect on thermosteic sea level rising for the year following the ENSO event.

## 5. Interannual sea level variability from tide gauges

Finally, we examine time series from tide gauge data to study the correlation between SOI and observed sea level on a longer time scale. Four tide gauges stations around the SCS are selected for this study. The four tide-gauge stations are: Quarry Bay (22°18′ N, 114°13′ E), ZHAPO (21°35′ N, 115°50′ E), VUNGTAU (10°20′ N, 107°04′ E), and KOTA KINABALU (5°59′ N, 116°04′ E), whose locations are denoted by a, b, c, and d in Fig. 1. Here the time series named as Quarry Bay is obtained from the data of both Quarry Bay (22°18′ N, 114°13′ E) and North Point (22°18′ N, 114°12′ E) in Hong Kong, which are from quite separate sites in areas of reclaimed land but which are geodetically connected to a common. The trends of the four tide gauges are 0.8±0.4 mm/yr, 2.2±0.4 mm/yr, 5.7±1.1 mm/yr and 5.0±1.6 mm/yr, respectively, as indicated in Fig. 10, where the error bars are the 95% confidence

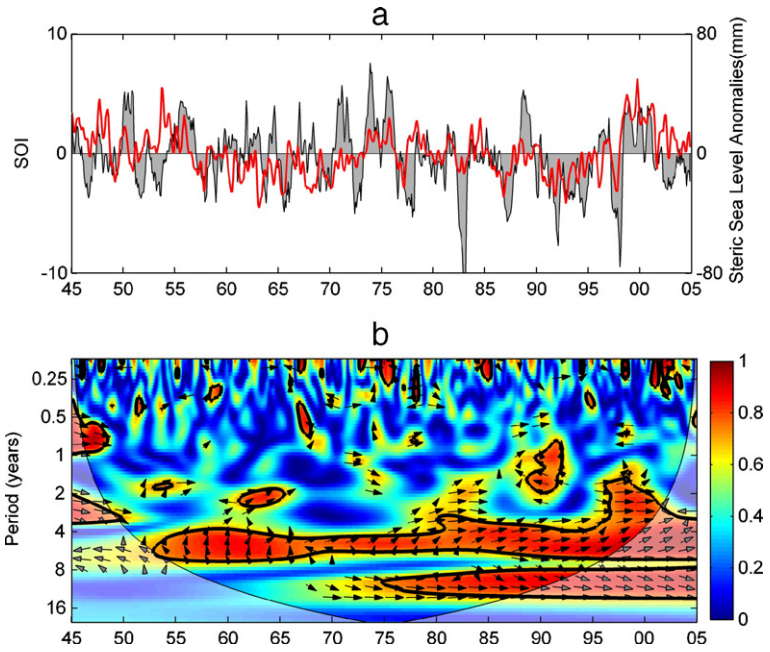


Fig. 9. Comparison of the SOI with the mean thermosteric sea level anomalies in the SCS (a) the time series of SOI (shaded curve) and the mean thermosteric sea level anomalies (red curve). The linear trend of thermosteric sea level has been removed and both time series are 3-month running means. (b) The wavelet coherence and phase relationship between SOI and the mean thermosteric sea level anomalies. The thick black contour is the 5% significance level and the cone of influence where edge effects might distort the picture is shown as a lighter shade. The vectors indicate the relative phase relationship (with in-phase pointing right, anti-phase pointing left, and SOI leading thermosteric sea level anomalies by 90° pointing straight up). (For interpretation of the references to colour in this figure legend, the reader is referred to the web version of this article.)

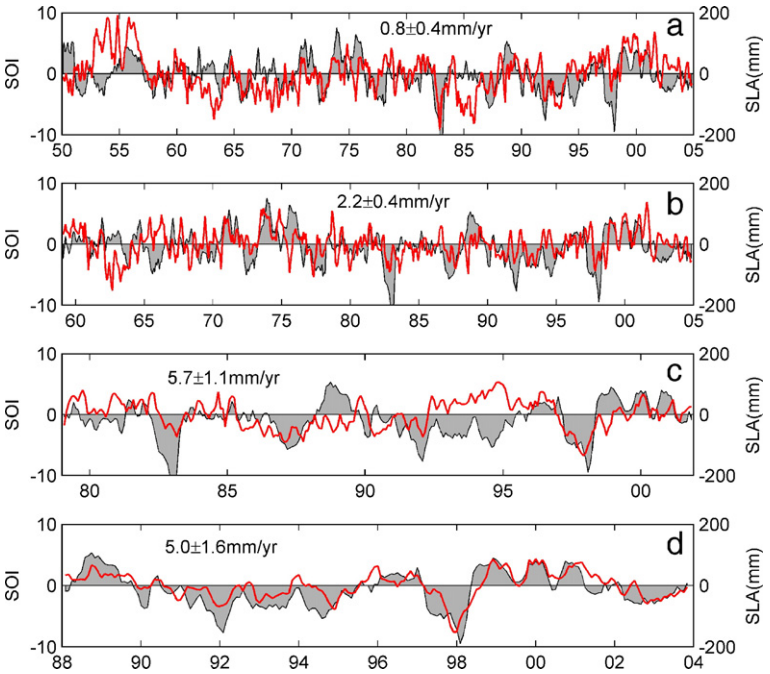


Fig. 10. Comparison of SOI (shaded curve) with sea level anomalies (red curve) observed by tide gauge at four stations: (a) Quarry Bay (22°18′ N, 114°13′ E), (b) ZHAPO (21°35′ N, 115°50′ E), (c) VUNGTAU (10°20′ N, 107°04′ E), (d) KOTA KINABALU (5°59′ N, 116°04′ E). The trends of the four tide gauges are also shown. (For interpretation of the references to colour in this figure legend, the reader is referred to the web version of this article.)

interval. All of the four stations show a rising trend though differences exist due to different time intervals and geographical locations. Fig. 10 also gives comparisons of SOI with the sea level anomalies observed by tide gauge at four stations after removing the seasonal signals and rising trend. As shown in Fig. 10, in many instances, sea level and SOI vary coherently, negative SOI (i.e. El Niño events) correlating with negative sea level and conversely. However, Fig. 10 also shows a few opposite examples, e.g. negative SOI during the period from 1994 to 1996 correlating with positive sea level anomalies at VUNG-TAU. Wavelet coherence analysis to SOI and sea level anomalies time series at these tide-gauge stations also reveal a high coherence between them (not shown). The interannual variability of sea level derived form tide gauges on a longer time interval confirms the results obtained from the relatively shorter altimeter observation.

## 6. Possible mechanisms of the interannual variability

### *6.1. Volume transports between the SCS and the adjacent oceans*

Since the SCS is a semi-closed ocean basin, seawater can exchange with the East China Sea, the Pacific Ocean, the Sulu Sea and the Java Sea through the Taiwan Strait, the Luzon Strait, the Balabec Strait and the Mindoro Strait, and the Karimata Strait, respectively, which may play important roles on sea level variation in the SCS. The total transport through Luzon Strait is essentially westward, and the mean value is estimated to be ranging from 0.5 to 10 Sv (Wyrtki, 1961; Metzger and Hurlburt, 1996; Qu, 2000; Lebedev and Yaremchuk, 2000; Chu and Li, 2000; Qu et al., 2000; Yaremchuk and Qu, 2004; Qu et al., 2004). With a set of numerical experiments, Metzger and Hurlburt (1996) noted that LST (Luzon Strait transport) is particularly sensitive to the model geometry. In this study, the seawater exchange between the SCS and the adjacent oceans is estimated based on SODA (Simple Ocean Data Assimilation) global reanalysis datasets (Carton and Giese, submitted for publication). This datasets are provided on a 0.5° × 0.5° horizontal resolution with 40 levels from 5 m to 5347 m, with the time interval from 1958 to 2004. The variables in the datasets include temperature, salinity, zonal and meridian velocities, wind stress and sea surface height. Here the zonal and meridian velocities are used to calculate the volume transport.

The annual cycles of the volume transports between the SCS and the adjacent oceans are shown in Fig. 11. In Fig. 11, the negative value denotes flowing in and the positive value denotes flowing out. In this study, 'EN' denotes the El Niño event, 'LN' denotes the La Niña event, and 'All' denotes the all years. Seawater enters into the SCS through the Luzon Strait over the whole year. The total transport through Luzon Strait has a maximum (3.1 Sv westward) in December and a minimum (0.74 Sv westward) in May. Most seawater entering into the SCS through the Luzon Strait flow out through the Karimata Strait. The volume transport through the Karimata Strait lags the LST by 1 month, with a maximum (2.6 Sv southward) in January and a minimum (0.37 Sv northward) in July, i.e. seawater enters into the SCS from June through August. The volume transports through the Balabec Strait and the Mindoro Strait are relatively weak. Seawater flows through the two straits into the SCS during the months from November through July, and flow out during other months. The volume transport through the Taiwan Strait is northward over the whole year with a peak 1.5 Sv in June, and it decreases from July to December and increases from January to June.

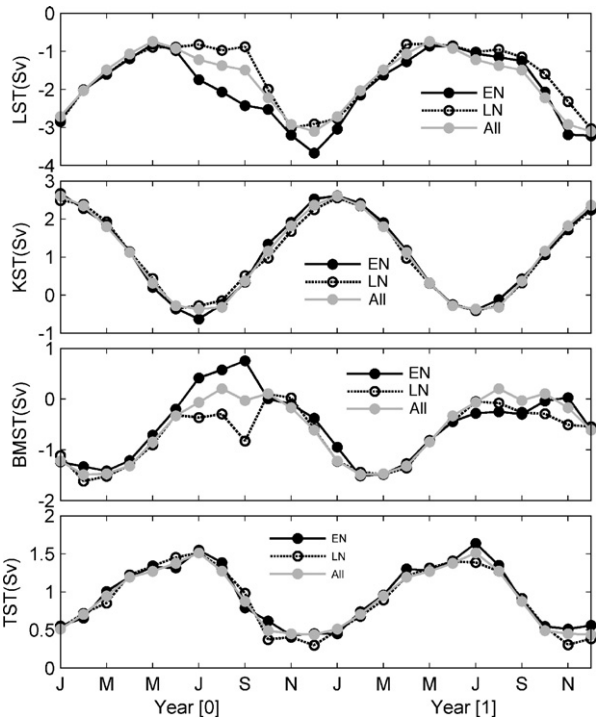


Fig. 11. Variations of Luzon Strait transport (LST) at 120.75° E, the Karimata Strait transport (KST) at 1.25° N, the Balabec Strait and the Mindoro Strait transport (BMST) and the Taiwan Strait transport (TST) at 24.75° N, with the time interval extending from 1958 to 2004. The Unit is Sv, with flowing in negative, flowing out positive. Note that [0] and [1] refer to the El Niño (La Niña) year and the subsequent year of the El Niño (La Niña) year, respectively. Geographic locations of these sections are shown in Fig. 1.

Table 2
List of El Niño and La Niña years from 1958 to 2004, which are taken from the following web site http://www.coaps.fsu.edu/products/jma_index.php. El Niño and La Niña years denote the months from October of the indicated year to September of the next year, e.g. the ENSO year 1997 starts October 1997 and ends September 1998

| | |
|---|---|
| El Niño | 1963, 1965, 1969, 1972, 1976, 1982, 1986, 1987, 1991, 1997, 2002 |
| La Niña | 1964, 1967, 1970, 1971, 1973, 1974, 1975, 1988, 1998, 1999 |

The volume transports are also grouped by El Niño and La Niña years (Table 2) and the monthly means are recalculated for each group. The mean patterns of volume transports related to ENSO are also shown in Fig. 11. In this study, [0] and [1] refer to the El Niño (La Niña) year and the subsequent year of the El Niño (La Niña) year, respectively. During July [0] through January [1], especially in the summer (July [0] through September [0]), the LST is larger than average during El Niño events by about 0.9 Sv and lower than average during La Niña events by about 0.6 Sv. In other months, LST during both El Niño and La Niña events does not normally differ from non-ENSO means. There are also striking responses of the Balabec Strait and Mindoro Strait transport to ENSO. More water flow out the SCS during the months of July [0] through September [0] when an El Niño is in its developing stage and seem to balance the increased LST. There are no apparent changes of Karimata Strait transport and Taiwan Strait transport during El Niño and La Niña conditions. As indicated by earlier studies (e.g. Qu, 2001), SST isotherms are oriented chiefly northeast–southwest, with SST decreasing from about 28.5° off Borneo to lower than 26.5° near the southern coast of China. That is to say, water enters the SCS with a lower temperature through the Luzon Strait and leave with higher temperature through the Karimata Strait, the Balabec Strait and the Mindoro Strait. At the developing stage of an El Niño event, the increased LST will produce a stronger than normal

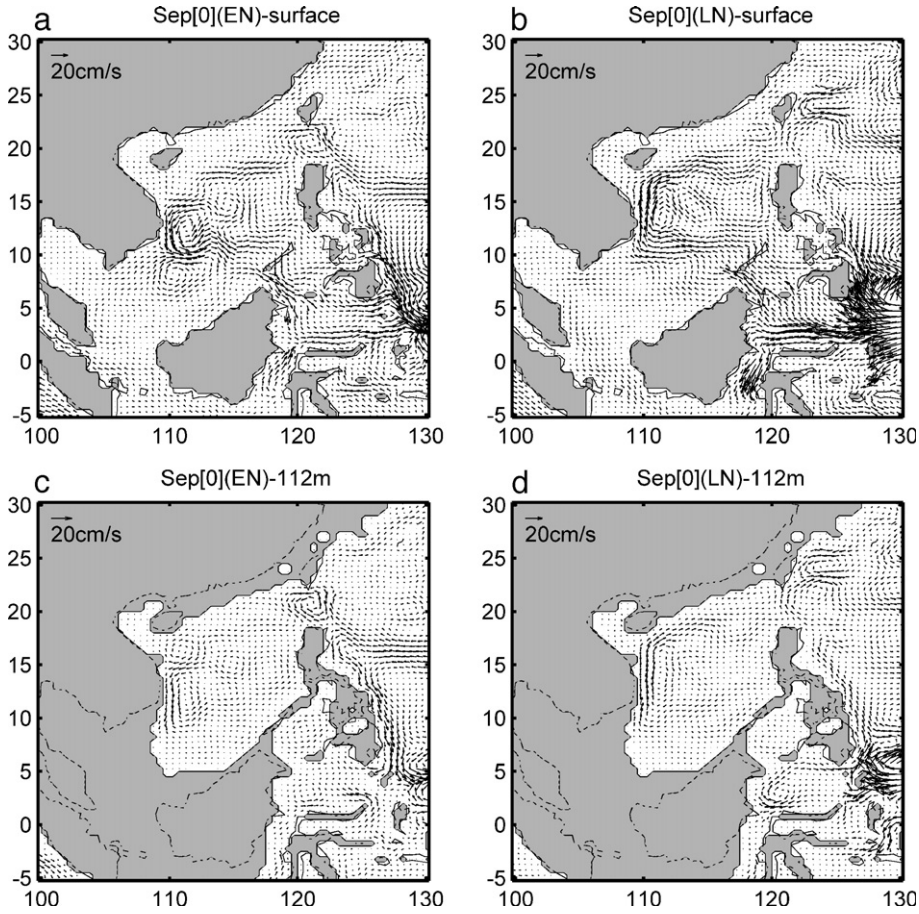


Fig. 12. The composite distributions of the oceanic circulation anomalies in September [0] based on SODA dataset(1958–2004) (a) El Niño years at surface, (b) La Niña years at surface, (c) El Niño years at 112 m depth, (d) La Niña years at 112 m depth.

cooling advection which eventually cools the SCS. This is consistent with earlier analysis (Qu et al., 2004). Meanwhile, volume transport through the Balabec Strait and the Mindoro Strait is larger than in normal years in the developing stage of an El Niño, thus more water with higher temperature flow out through the two straits, which is apt to cool the SCS. The final effect of these processes is to form negative sea level anomalies when an El Niño happens. The situation is reversed during La Niña years.

### 6.2. Oceanic circulation

Fig. 12 shows the mean oceanic circulation anomalies in September [0] at surface and 112 m depth for El Niño (EN) and La Niña (LN) based on the SODA dataset. Here September [0] denotes the September in El Niño (or La Niña) years. Obviously, there is an anomalous anti-clockwise circulation in September [0] when an El Niño is in its developing stage, and this anomalous anti-clockwise circulation can extend to the depth deeper than 100 m (Fig. 12c). The anti-clockwise circulation indicates a divergence in the central deep basin. Cold water is pumped from the deep layer to the surface and are further driven to the coastal areas due to the circulation system. So sea level in the deep basin should be lower than the normal during and after the developing stage of an El Niño.

Fig. 13 shows the composite distributions of sea level anomalies in September [0] based on SODA dataset and altimeter observations, respectively. Both maps from reanalysis data and observation show that sea level anomalies in the deep basin are apparently lower than the normal during El Niño events and higher during La Niña

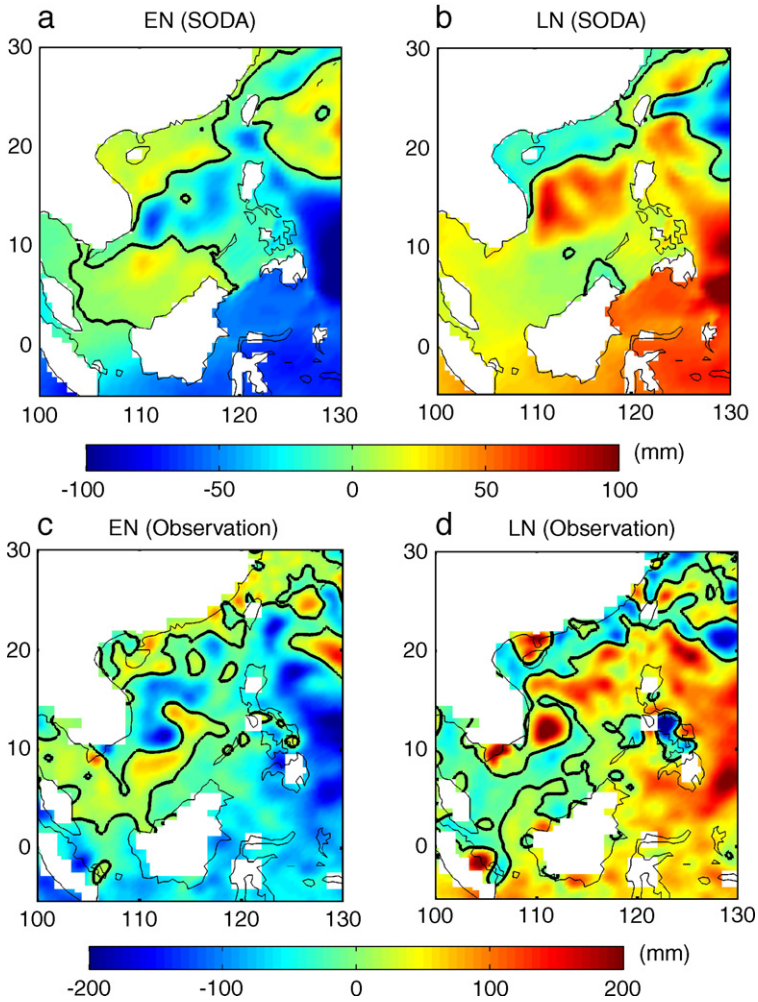


Fig. 13. The composite distributions of sea level anomalies in September [0] from SODA (1958–2004) and Altimeter Observations (1993–2004) (a, c) El Niño years, (b, d) La Niña years. The thick black contour is the zero line.

events. The mechanism may be the southwesterly monsoon. In summer when an El Niño event is in its developing stage, an anomalous cyclonic circulation exists over the western Pacific, which indicates a weak western Pacific subtropical high (Huang et al., 2004). This is apt to form cyclonic wind anomalies over the SCS, which will induce seawater divergence anomalies in the SCS, and eventually anti-clockwise oceanic circulation anomalies. Meanwhile, the increased Kuroshio intrusion is apt to enhance the north branch of the anti-clockwise oceanic circulation, which may also play a role for the forming of the anomalous anti-clockwise circulation (Fig. 12a, c). The divergence in the central deep basin may also explain why seawater temperature at 100 m depth is abnormally cold before and during the mature phase of El Niño, since the thermocline was shoaled due to Ekman pumping. In the preceding summer of a La Niña, the situation seems reversed. An anomalous clockwise circulation is formed in the central SCS (Fig. 12b, d), which represents seawater convergence there. A consequence of the convergence is that it piles up warm water there. The sinking of the warm water will deepen the mixed layer depth and the ocean is apt to capture more heat during La Niña years, and sea level will rise then.

When an El Niño event happens, atmospheric convective activities are enhanced over the equatorial central and eastern Pacific and weakened over the tropical western Pacific. The anomalous convection over the central Pacific strengthens the local Hadley cell, and also produces anomalous subsidence over Indonesia (via the altered Walker cell), thereby weakens the Hadley cell in this remote region (Klein et al., 1999; Wang, 2002). Corresponding to the anomalous sinking are anomalous anticyclones above the off-equatorial western Pacific during and after the mature phase of El Niño (Weisberg and Wang, 1997; Wang et al., 1999; Huang et al., 2004). The South China Sea lies near the region of descent in the anomalous Walker cell. During the mature phase of an El Niño (November to January) there are anomalous south or southwest winds in the South China Sea (not shown). This anomalous circulation opposes the mean wintertime northeast flow which can transport cold and dry air. Thus it will induce a reduction in the mean surface wind speed and the occurrence of cold air breaks. Accordingly, the latent and sensible heat flux will be significantly reduced (Klein et al., 1999). So SST is abnormally high during and after the mature phase of El Niño. Usually, there is a La Niña following the El Niño, for example the 1997 El Niño and the 1998 La Niña. The warmer SST after the mature phase of El Niño may also play a role in sea level rising during La Niña years.

### 6.3. Water mass exchange through the water cycle

For the water mass exchange in the SCS, not only its annual signal is very strong (with an amplitude of 63 mm), but also its interannual variability plays a significant contribution to the observed sea level variation. Fig. 14 shows the interannual variation of the mass exchange (i.e. altimeter height minus thermosteric height) after removing the seasonal signals (annual and semiannual signals), and the SOI is also superimposed. The interannual variation of the mass exchange is closely related to SOI (ENSO). The correlation between them reaches 0.42, with the SOI leading the mass exchange by about 4 months. Less water enter into the SCS during El Niño years, for example the 1997–1998 El Niño year. A reverse situation takes place during La Niña years, with more water entering into the SCS, such as the 1998–1999 and 1999–2000 La Niña years. To further understand the mass exchange in the SCS, we try to investigate the precipitation variation over the SCS (1.25°–23.75° N, 101.25°–121.25° E), as a part of the mass exchange. The CMAP (CPC Merged Analysis of Precipitation) precipitation data are used here. This dataset consists of monthly averaged precipitation rate values (mm/day), with a temporal coverage from 1979 to 2006. The precipitation data are obtained from 5 kinds of satellite estimates (GPI, OPI, SSM/I scattering, SSM/I emission and MSU) (Xie and Arkin, 1997).

Fig. 15a shows the mean precipitation rate over the SCS and the corresponding annual fits are superimposed. The annual signal of the precipitation rate has an amplitude of 3.2 mm/day, with a maximum in August and a minimum in February. Fig. 15b shows the interannual variation of the precipitation rate after removing the seasonal signals (annual and semiannual signals). The temporal correspondence of precipitation rate with ENSO is striking. The correlation between the precipitation rate and SOI is 0.55, with SOI leading the precipitation by 1 month. In general, the precipitation rate is lower during

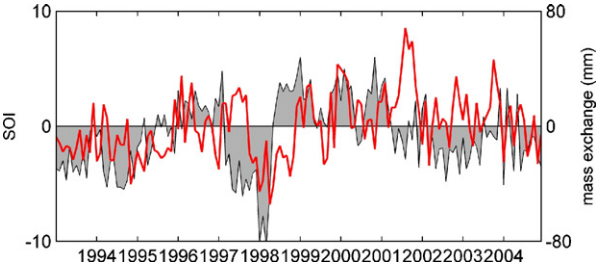


Fig. 14. Comparison of the SOI (shaded curve) with the mass exchange (i.e.altimeter observed sea level minus thermosteric sea level) after removing the seasonal signals (annual and semiannual signals).

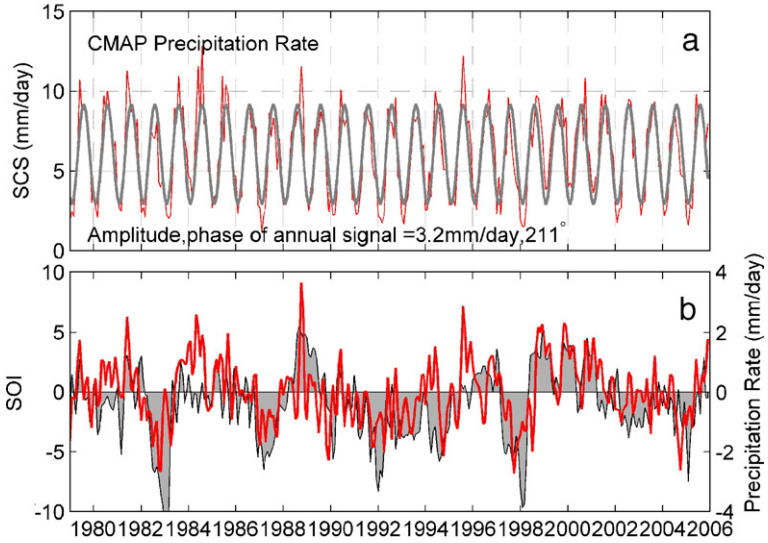


Fig. 15. (a) The CMAP precipitation rate over the SCS (red line) and the annual fits (gray line); (b) Comparison of the SOI (shaded curve) with the precipitation rate after removing the seasonal signals (annual and semiannual signals). (For interpretation of the references to colour in this figure legend, the reader is referred to the web version of this article.)

El Niño years and higher during La Niña years. It is worth to note that interannual variation of mass exchange is dominantly controlled by the interannual variation of precipitation. Its peak to peak amplitude is about 4 mm/day. This will account for about 60 mm negative sea level anomalies during El Niño years. During El Niño years, there is an anomalous subsidence of the Walker cell over the western equatorial Pacific. It is not surprising to see that the reduced convection over there decreases the cloud cover, which is apt to reduce the precipitation. The situation is reversed during La Niña years, convection is enhanced over the western equatorial Pacific and the precipitation rate is high over the SCS.

Note that although the thermosteric sea level falls (rises) during El Niño (La Niña) years, it varies about 3 months leading the SOI (see Fig. 9 and Table 1). The fall of thermosteric sea level before and during the mature phase of El Niño does play an important role for the observed sea level fall. However, other factors should account for the following continuous fall of sea level, since the observed sea level reaches its minimum with a lag of 4 months behind the SOI (See Table 1). Mass exchange through the water cycle plays a role to balance this. Fewer water enter into the SCS during El Niño years and more water enter into the SCS during La Niña years. That is to say, the thermosteric contributes a lot for the sea level fall in the developing stage of El Niño, while the mass exchange, mainly due to precipitation, plays a more significant role for the following continuous negative sea level anomalies.

## 7. Summary

Based on altimeter observed sea level data, Ishii temperature data and tide gauge data, this study provides a detailed description of interannual variability of observed and thermosteric sea level in the SCS. The conclusions are summarized as follows.

Sea level anomalies in the SCS are dominated by interannual fluctuations. Interannual variation of observed sea level shows a good correspondence with ENSO. The mean sea level anomalies are negative during El Niño years and positive during La Niña years. EOF analysis of the low-pass filtered sea level anomalies also reveals that the sea level has a response to ENSO. The first EOF mode related to ENSO occupied 62% of the total variance. Sea level falls synchronously during El Niño years over the whole sea, and rises during La Niña years.

An ‘enigma’ that the SST and the sea level over the SCS have almost inverse response to ENSO is revealed. While SST reaches its maximum with a lag of 5 months behind the mature phase of El Niño, sea level reaches its minimum with a lag of 4 months. Such an ‘enigma’ is revealed by calculating the heat expansion of seawater in the 0–700 m layer. The SST is mainly determined by seawater temperature in the surface layer. The sea level is related to the heat expansion of seawater in all the layers. This study has indicated that the correlation between SOI and seawater temperature in the upper 75 m is negative and that in the intermediate layers

(deeper than 75 m) is positive (see Fig. 7). Comparison of the SOI with the seawater temperature anomalies at 100 m depth in the SCS implies that the seawater temperature anomalies at intermediate layers have a synchronous correspondence with SOI (see Fig. 8) and also the thermosteric sea level anomalies (see Fig. 9). This suggests that the thermosteric sea level anomalies are dominantly controlled by seawater temperature anomalies of the intermediate layers.

During July [0] through September [0] when an El Niño is in its developing stage, more cold water enter into the SCS through the Luzon Strait, and more warm water flow out the SCS through the Balabec Strait and the Mindoro strait. A stronger than normal cooling advection will play a negative role in sea level variation over the SCS. Meanwhile, there is an anomalous weak Western Pacific high at the developing stage of an El Niño (Huang et al., 2004). This will alter the wind field over the SCS, and an anomalous anti-clockwise oceanic circulation is formed over the SCS, indicating an abnormally divergence over the central SCS. Sea level there is abnormally lower than the normal during El Niño conditions and higher during La Niña conditions. The anomalous divergence will also explain why seawater temperature at 100 m depth is anomalously cold before and during the mature phase of an El Niño, since the thermocline was shoaled due to Ekman pumping. The anomalous anti-clockwise circulation plays a negative role in the thermosteric sea level variation and eventually the observed sea level. The situation is reversed during La Niña years.

During El Niño, the atmospheric convective activity in the equatorial Pacific shifts eastward and an anomalous descent is formed over the tropical Indo–western Pacific (Klein et al., 1999; Wang, 2002). Corresponding to the anomalous descent are anomalous anticyclones above the off-equatorial western Pacific during and after the mature phase of El Niño (Weisberg and Wang, 1997; Wang et al., 1999). The SCS locates near the region of anomalous descent motion. It is unsurprising that the reduced convection decreases the cloud cover and eventually reduces the precipitation during El Niño years. The decreased precipitation plays a significant role for the continuous negative sea level anomalies, which will account for about 60 mm sea level fall during El Niño years. On the other hand, the anomalous descent motion, associated with the anomalous anticyclone in north western Pacific will alter the surface wind, humidity, air temperature and cloud cover over the SCS, which in turn increase the net heat flux entering the SCS, thereby leading to enhanced SST (Klein et al., 1999; Wang et al., 2006). Usually, there is a La Niña following the El Niño, for example, the 1997 El Niño and the 1998 La Niña. The abnormally warm SST after the mature phase of El Niño may also play a role for the sea level rise during La Niña years.

## Acknowledgement

This study was supported by the National High Technology Development Project of China under Grant 863-2001AA633030 and 2005AA604150.

## References

Boyer, T.P., Conkright M.E., Antonov J.I., Baranova O.K., Garcia H., Gelfed R., Johnson D., Locarnini R., Murphy P., Brien T.O., Smolyar I., Stephens C., 2001. World Ocean Database 2001, Volume 2: Temporal Distribution of Bathythermograph Profiles. NOAA Atlas NESDIS 43. 119pp., CD-ROMs, U.S. Government Printing Office, Washington, D.C.

Chu, P.C., Li, R., 2000. South China Sea isopycnal-surface circulation. J. Phys. Oceanogr. 30, 2419–2438.

Carton, J.A., Giese, B.S., submitted for publication. SODA: A reanalysis of Ocean Climate. J. Geophys. Res.

Ducet, N., Le Traon, P.Y., Reverdin, G., 2000. Global high resolution mapping of ocean circulation from TOPEX/Poseidon and ERS-1 and -2. J. Geophys. Res. 105 (C8), 19477–19478.

Gill, A.E., 1982. Atmosphere–Ocean Dynamics. Academic Press, San Diego. 662pp.

Grinsted, A., Moore, J.C., Jevrejeva, S., 2004. Application of the cross wavelet transform and wavelet coherence to geophysical time series. Nonlinear Process in Geophysic 11, 561–566.

Ho, C.R., Zheng, Q., Soong, Y.S., Kuo, N.J., Hu, J.H., 2000a. Seansonal variability of sea surface height in the South China Sea observed with TOPEX/Poseidon altimeter data. J. Geophys. Res. 105 (C6), 13981–13990.

Ho, C.R., Kuo, N.J., Zheng, Q., Soong, Y.S., 2000b. Dynamically active areas in the South China Sea detected from TOPEX/Poseidon satellite altimeter data. Remote Sens. Environ. 71, 320–328.

Hu, J., Kawamura, H., Hong, H., Kobashi, F., Wang, D., 2001. 3~6 months variation of sea surface height in the South China Sea and its adjacent ocean. J. Oceanogr. 57 (1), 69–78.

Huang, R., Chen, W., Yang, B., Zhang, R., 2004. Recent advances in studies of the interaction between the East Asian winter and summer monsoons and ENSO cycle. Adv. Atmos. Sci. 21 (3), 407–424.

Hwang, C., 2001. Interannual variation of sea level of South China Sea and its relationship with ENSO. Paper Presented at the ASPG Fourth Workshop, ASPG Management board and the Shanghai Astronomical Observatory, CAS, Shanghai, P.R. China, 14–19 May.

Ishii, M., Kimoto, M., Kachi, M., 2003. Historical ocean subsurface temperature analysis with error estimates. Mon. Weather Rev. 131, 51–73.

Ishii, M., Shouji, A., Sugimoto, S., Matsumoto, T., 2005. Objective analyses of SST and marine meteorological variables for the 20th century using COADS and the Kobe Correction. Int. J. Climatol. 25, 865–879.

Ishii, M., Kimoto, M., Sakamoto, K., Iwasaki, S.-I., 2006. Steric sea level changes estimated from historical ocean subsurface temperature and salinity analyses. J. Oceanogr. 62 (2), 155–170.

Klein, S.A., Soden, B.J., Lau, N.C., 1999. Remote sea surface temperature variations during ENSO: evidence for a tropical atmospheric bridge. J. Clim. 12, 917–932.

Lebedev, K.V., Yaremchuk, M.I., 2000. A diagnostic study of the Indonesian throughflow. J. Geophys. Res. 105, 11243–11258.

Li, L., Xu, J., Jing, C., Wu, R., Guo, X., 2003. Annual variation of sea surface height, dynamics topography and circulation in the South China Sea. Sci. China (Ser. D) 46 (2), 127–138.

Liu, Q., Jia, Y., Wang, X., Yang, H., 2001. On the annual cycle characteristics of the sea surface height in South China Sea. Adv. Atmos. Sci. 18 (4), 613–622.

Lombard, A., Cazenave, A., Le Traon, P.Y., Ishii, M., 2005. Contribution of thermal expansion to present-day sea-level change revisited. Glob. Planet. Change 47, 1–16.

Metzger, E.J., Hurlburt, H.E., 1996. Coupled dynamics of the South China Sea, the Sulu Sea, and the Pacific Ocean. J. Geophys. Res. 101, 12331–12352.

Preisendorfer, R., 1988. Principal Component Analysis in Meteorology and Oceanography. Elsevier, New York. 425pp.

Qu, T., 2000. Upper-layer circulation in the South China Sea. J. Phys. Oceanogr. 30, 1450–1460.

Qu, T., 2001. Role of ocean dynamics in determining the mean seasonal cycle of the South China Sea surface temperature. J. Geophys. Res. 106, 6943–6955.

Qu, T., Mitsudera, H., Yamagata, T., 2000. Intrusion of the North Pacifica waters into the South China Sea. J. Geophys. Res. 105, 6415–6424.

Qu, T., Kim, Y.Y., Yaremchuk, M., Tozuka, T., Ishida, A., Yamagata, T., 2004. Can Luzon strait transport play a role in conveying the impact of ENSO to the South China Sea? J. Clim. 17, 3644–3657.

Trenberth, K.E., 1984. Some effects of finite sample size and persistence on meteorological statistics. Part I: autocorrelations. Mon. Weather Rev. 112, 2359–2368.

Wyrtki, K., 1961. Physical oceanography of the southeast Asian waters. Naga Rep., vol. 2. Scripps Institution of Oceanography, La Jolla, CA. 195pp.

Weisberg, R.H., Wang, C., 1997. A western Pacific oscillator paradigm for the El Niño–Southern Oscillation. Geophys. Res. Lett. 24, 779–782.

Wang, C., Weisberg, R.H., Virmani, J.I., 1999. Western Pacific interannual variability associated with the El Niño–Southern Oscillation. J. Geophys. Res. 104, 5131–5149.

Wang, W., Wang, D., Qi, Y., 2000. Large scale characteristics of interannual variability of sea surface temperature in the South China Sea. Acta Oceanol. Sin. 22, 8–16.

Wang, C., 2002. Atmospheric circulation cells associated with the El Niño–South Oscillation. J. Clim. 15, 399–419.

Wang, C., Wang, W., Wang, D., Wang, Q., 2006. Interannual variability of the South China Sea associated with El Niño. J. Geophys. Res. 111, C030203. doi:10.1029/2005JC003333.

Xie, P., Arkin, P.A., 1997. Global precipitation: a 17-year monthly analysis based on gauge observations, satellite estimates, and numerical model outputs. Bull. Am. Meteorol. Soc. 78, 2539–2558.

Yaremchuk, M., Qu, T., 2004. Seasonal variability of the large scale currents near the coast of the Philippines. J. Phys. Oceanogr. 34, 844–855.